Fluid-mechanical interaction of flexible bacterial flagella by the immersed boundary method

Sookkyung Lim and Charles S. Peskin

Phys. Rev. E **85**, 036307 — Published 19 March 2012

DOI: 10.1103/PhysRevE.85.036307

Fluid-mechanical interaction of flexible bacterial flagella by the immersed boundary method

Sookkyung Lim*

Department of Mathematical Sciences, University of Cincinnati,

4199 French Hall West, Cincinnati, OH 45221

Charles S. Peskin†

Courant Institute of Mathematical Sciences,

New York University, 251 Mercer St. New York, NY 10012

Abstract

Flagellar bundling is an important aspect of locomotion in bacteria such as *Escherichia coli*. To study the hydrodynamic behavior of helical flagella, we present a computational model that is based on the geometry of the bacterial flagellar filament at the micron scale. We consider two model flagella, each of which has a rotary motor at its base with the rotation rate of the motor set at 100Hz. Bundling occurs when both flagella are left-handed helices turning counterclockwise (when viewed from the non-motor end of the flagellum looking back towards the motor) or when both flagella are right-handed helices turning clockwise. Helical flagella of the other combinations of handedness and rotation direction do not bundle.

* Corresponding author. sookkyung.lim@uc.edu

† peskin@cims.nyu.edu

I. INTRODUCTION

Bacteria such as *Escherichia coli* and *Salmonella typhimurium* swim in an aqueous environment by rotating their helical flagella. Each flagellar filament is driven by a rotary motor embedded in the cell surface. The motor can turn either clockwise (CW) or counterclockwise (CCW), where the terms CW and CCW refer to an observer who views the flagella from outside the bacterium. The rotation of the motors leads the cell either to *run* or to *tumble*. The runs are driven by flagellar bundling; all of the flagellar motors turn CCW and the flagella coalesce into a superflagellum. When at least one of the motors changes its direction of rotation from CCW to CW the bundle unravels and the flagella fly apart; the cell then tumbles [1–3].

Studies of the swimming mechanism of bacteria have been done by many investigators [4–13]. Both experimental and theoretical studies have underscored the complexity of flagellar geometry during swimming. In particular, the diameter (thickness) of the flagellar filament, 20nm, is very small in comparison to other scales such as filament length, $5 \sim 10\mu$m [3]. Furthermore, the rotation rate of the motor is relatively high (100 Hz) [1], and the rotating helices go through polymorphic transformations (local changes in helical wavelength, helical diameter, and handedness). It is known that polymorphic transformations can be triggered by the hydrodynamic interaction of flagella and by changes in direction of rotation, pH, temperature, salinity, or mechanical forces [5, 6, 14–18]. It is believed that such polymorphism plays a role in the unbundling of flagella, which occurs during the transition from a run to a tumble. In the present work, however, polymorphic transitions are not included. Each of our model flagella has a unique preferred helical configuration, and is not bistable or multistable. Our modeling framework can be generalized, however, to allow for polymorphism, so this will be mentioned as a future application of our methodology.

The energetic benefit of bundling (if any) is not addressed in the present paper. One may speculate that an energetic benefit exists on the basis of the demonstration of such a benefit by G.I.Taylor [19] for the swimming of parallel synchronized waving sheets, with application to the swimming of spermatozoa. Note, however, that Taylor was concerned in that paper with planar motion, not with helical waves. In a subsequent paper [20], Taylor does address the problem of helical motion (but of a single flagellum) and there he describes a mechanical model with a rotating rubber-band driven motor, which he regards as un-biological because

of its rotary nature. As we now know, the bacterial flagellar motor is indeed rotary, so Taylor's mechanical model was better than he imagined, although applicable to bacteria and not to sperm.

In this paper we study first a single flagellum, and then a pair of flagella that rotate side by side in a viscous fluid. Our model flagella have a definite handedness and are not capable of polymorphic transformation. Each flagellum has a motor at one end which turns at a specified rate in a specified direction. The motor end of the flagellum is held at a fixed location in space with a prescribed direction for the tangent to the centerline of the flagellum at the motor location. The model flagella are immersed in a periodic box of viscous incompressible fluid, in which there are no boundaries other than the flagella themselves.

In this work we use the Kirchhoff theory of thin rods in the mathematical modeling of flagella. The Kirchhoff model of a thin elastic rod that resists bending and twisting involves a three-dimensional space curve together with an orthonormal triad (material frame) at each point of that curve. Comparison between the orientations of nearby triads indicates how much the filament bends or twists. Furthermore, we prescribe intrinsic curvature and intrinsic twist such that the equilibrium configuration of the rod is helical in the absence of any applied forces and moments [21, 22]. The resulting Kirchhoff rod model is immersed in a viscous incompressible fluid to study the interaction of one flagellum with itself and of two flagella spinning side by side.

Our framework for fluid-structure interaction is the immersed boundary (IB) method. The original IB method was introduced by Peskin in the 1970s to study flow patterns around heart valves. It has been improved and applied to biofluid mechanical problems, for example, animal locomotion, insect flight, blood clotting, and valveless pumping applicable to CPR (cardiac pulmonary resuscitation) [23–30].

Some special features of the IB method used here [22, 31] are that: (a) the interaction of an immersed filament with a fluid involves not only translation of the immersed boundary points of the filament at the local fluid velocity, but also rotation of the associated triads at the local fluid angular velocity, and (b) that the rod applies torque as well as force to the fluid. Two additional special features not used in [22, 31] are that: (c) a provision for slip velocity, and likewise for slip angular velocity, of the immersed filament relative to the velocity and angular velocity of the surrounding fluid, and (d) an application of the repulsive force between flagella that does not allow any two points of the flagellar filaments

to approach closer than the specified distance. Provision for slip and the repulsive force are needed only because we cannot afford to make the fluid grid fine enough to resolve the flow pattern that occurs within a flagellar bundle. This flow pattern has to be non-trivial. It cannot approximate a rigid-body rotation, since that would imply that the flagella of the bundle, which are anchored at their motor ends, would have to wind progressively around each other until ultimately they would have to break. (We thank Philip Holmes for pointing out this fundamental problem.) By allowing for relative slip between the model flagella and the model fluid and for the repulsiveness between flagella, we are able to avoid the extremely close approach during bundling that could otherwise lead the model flagella to pass through each other.

The mathematical formulation of our problem will be described in Section II. We consider helical flagellar filaments rotated at a specified frequency and investigate their behavior in a viscous incompressible fluid. Our main interest will be in the hydrodynamic interaction between two flagella. Simulation results will be presented and discussed in Section III.

II. MODEL

The formulation of the problem as stated in this section is similar to that used in [31], in which the fluid-structure interaction of a closed rod with bend and twist was studied. The principal differences from that work are that the rod (here, a model flagellum) is no longer closed, that it has a motor at one end, and that its relaxed configuration is helical rather than straight.

The reference configuration (which we also use as an initial condition) of our model flagellum is that of a straight non-twisted rod. As will be seen below, this is *not* an equilibrium configuration of the rod, but it is a convenient reference configuration nonetheless. The reference/initial configuration is as follows:

$$\mathbf{X}(s,0) = (0,0,s), \tag{1}$$

$$\mathbf{D}^1(s,0) = (1,0,0), \tag{2}$$

$$\mathbf{D}^2(s,0) = (0,1,0), \tag{3}$$

$$\mathbf{D}^3(s,0) = (0,0,1), \tag{4}$$

where s such that $0 \leq s \leq l$ is a Lagrangian parameter which measures arclength in the

reference configuration but is not necessarily equal to arclength otherwise. Here $\mathbf{X}(s,t)$ denotes the centerline of the flagellar filament and $\{\mathbf{D}^1(s,t), \mathbf{D}^2(s,t), \mathbf{D}^3(s,t)\}$ denotes the collection of orthonormal triads along the filament. We regard one of the end points of each flagellum, located at $s = 0$, as a motor point, and we fix the position of that point in space.

To simulate a motor at $s = 0$, we rotate the triad located there at a prescribed angular velocity ω. Unless otherwise indicated $|\omega| = 2\pi(100)/\text{s}$, so that the motor rotates at 100Hz. Thus, our constraints at the motor end of the flagellum take the form:

$$\mathbf{X}(0,t) = \mathbf{X}_0, \tag{5}$$

$$\mathbf{D}^1(0,t) = (\cos(\omega t), \sin(\omega t), 0), \tag{6}$$

$$\mathbf{D}^2(0,t) = (-\sin(\omega t), \cos(\omega t), 0), \tag{7}$$

$$\mathbf{D}^3(0,t) = (0,0,1). \tag{8}$$

Note that $\omega > 0$ corresponds to counterclockwise (CCW) rotation, whereas $\omega < 0$ corresponds to clockwise (CW) rotation, assuming that the flagellum is viewed looking back towards $s = 0$ from a location at which $s > 0$, as is the case when the flagellum is viewed from outside the bacterium.

The Kirchhoff rod model that we use is defined by an elastic energy of the form:

$$E = \frac{1}{2}\int \left[a_1 \left(\frac{d\mathbf{D}^2}{ds} \cdot \mathbf{D}^3 - \kappa_1 \right)^2 + a_2 \left(\frac{d\mathbf{D}^3}{ds} \cdot \mathbf{D}^1 - \kappa_2 \right)^2 + a_3 \left(\frac{d\mathbf{D}^1}{ds} \cdot \mathbf{D}^2 - \tau \right)^2 \right.$$
$$\left. + b_1 \left(\mathbf{D}^1 \cdot \frac{d\mathbf{X}}{ds} \right)^2 + b_2 \left(\mathbf{D}^2 \cdot \frac{d\mathbf{X}}{ds} \right)^2 + b_3 \left(\mathbf{D}^3 \cdot \frac{d\mathbf{X}}{ds} - 1 \right)^2 \right] ds, \tag{9}$$

where a_1 and a_2 are the bending moduli of the rod about $\mathbf{D}^1$ and $\mathbf{D}^2$, respectively, and a_3 is the twisting modulus of the rod. Note that $a_1 = a_2$ in the case of a rod with a circular cross section and axially symmetric material properties, which we assume here. The parameters b_1 and b_2 are the shear force constant and b_3 is the stretch force constant. The vector $(\kappa_1, \kappa_2, \tau)$, where $\kappa_1, \kappa_2 > 0$, is called the intrinsic twist vector. It determines the intrinsic helical shape of the model flagellum, as discussed more fully below.

The moduli a_1, a_2, and a_3 are the standard parameters of the Kirchhoff rod model. The moduli b_1, b_2, and, to a lesser extent, b_3, are non-standard; they are penalty parameters which, when chosen large, produce an energy function which tends to enforce the following two conditions: First, when b_1 and b_2 are large, the terms in the energy function in which they appear produce a strong tendency to align the vector $\mathbf{D}^3$ with the tangent vector $\partial\mathbf{X}/\partial s$

to the curve $\mathbf{X}(s,t)$ that defines the centerline of the rod. In the standard Kirchhoff rod model, this alignment occurs by definition, but we cannot make such a definition here, since we want $\{\mathbf{D}^1, \mathbf{D}^2, \mathbf{D}^3\}$ to rotate at the local angular velocity of the fluid. Thus, we need a *physical* mechanism to maintain, albeit only approximately, the desired alignment. The second condition, which tends to be well maintained when b_1, b_2, and b_3 are all large, is that the parameter s should measure arclength along the flagellum, i.e., that $|\partial\mathbf{X}/\partial s| = 1$. Since s is a Lagrangian parameter, this is equivalent to saying that the flagellum is inextensible. Again, since each point of the flagellum is supposed to move at the local fluid velocity, we cannot impose the constraint in inextensibility by fiat, but need a *physical* mechanism to enforce it to a sufficiently good approximation. For further details on this penalty form of the Kirchhoff rod model, see [31].

The energy function stated above generalizes the one used in [31] by the inclusion of the parameters κ_1, κ_2, and τ, which give the rod a helical intrinsic shape. When these parameters are not all zero, the straight non-twisted reference configuration defined above is *not* an equilibrium configuration of the rod. More specifically, $\kappa = \sqrt{\kappa_1^2 + \kappa_2^2}$ is the *intrinsic curvature* and τ is the *intrinsic twist*. The sign of the intrinsic twist τ determines the handedness of the helix, positive values for right-handedness and negative values for left-handedness, see [22] for further details.

The intrinsic curvature and twist determine the equilibrium geometry of the helix through the parameters r and p defined as follows [12, 21]:

$$r = \frac{\kappa}{\kappa^2 + \tau^2}, \quad p = \frac{\tau}{\kappa^2 + \tau^2}. \tag{10}$$

The significance of these parameters is that $2\pi r$ is the circumference of the cylinder on which the helix lies, and $2\pi p$ is the axial distance that is traversed during one turn of the helix.

The energy function described above has only a global minimum corresponding to a particular helical configuration, depending on the parameters κ and τ, and no other local minima. The filament described by this energy function is therefore monostable – it does not exhibit polymorphism. We note, however, that this type of model can easily be generalized to allow for polymorphisms of different kinds through the use of energy functions with two or more local minima. As a simple example of this, one could replace the term involving a_3 in equation (9) by the following:

$$a_3 \left(\left| \frac{d\mathbf{D}^1}{ds} \cdot \mathbf{D}^2 \right| - \tau \right)^2. \tag{11}$$

In this case, τ is a positive parameter defining the magnitude of the twist, and there are two minima corresponding to helices that differ in handedness only.

Having defined the model flagellum itself by the Kirchhoff rod energy function stated above, we now proceed to state the coupled system of equations that describe such a flagellum in a viscous incompressible fluid:

$$\rho\left(\frac{\partial \mathbf{u}}{\partial t} + \mathbf{u}\cdot\nabla\mathbf{u}\right) = -\nabla p + \mu\nabla^2\mathbf{u} + \mathbf{f}^{\mathrm{b}}, \tag{12}$$

$$\nabla\cdot\mathbf{u} = 0, \tag{13}$$

$$0 = \mathbf{f} + \frac{\partial \mathbf{F}}{\partial s}, \tag{14}$$

$$0 = \mathbf{n} + \frac{\partial \mathbf{N}}{\partial s} + \frac{\partial \mathbf{X}}{\partial s}\times\mathbf{F}, \tag{15}$$

$$\mathbf{F} = F^1\mathbf{D}^1 + F^2\mathbf{D}^2 + F^3\mathbf{D}^3, \tag{16}$$

$$\mathbf{N} = N^1\mathbf{D}^1 + N^2\mathbf{D}^2 + N^3\mathbf{D}^3, \tag{17}$$

$$N^1 = a_1\left(\frac{\partial \mathbf{D}^2}{\partial s}\cdot\mathbf{D}^3 - \kappa_1\right), N^2 = a_2\left(\frac{\partial \mathbf{D}^3}{\partial s}\cdot\mathbf{D}^1 - \kappa_2\right), N^3 = a_3\left(\frac{\partial \mathbf{D}^1}{\partial s}\cdot\mathbf{D}^2 - \tau\right), \tag{18}$$

$$F^1 = b_1\mathbf{D}^1\cdot\frac{\partial \mathbf{X}}{\partial s}, \quad F^2 = b_2\mathbf{D}^2\cdot\frac{\partial \mathbf{X}}{\partial s}, \quad F^3 = b_3\left(\mathbf{D}^3\cdot\frac{\partial \mathbf{X}}{\partial s} - 1\right), \tag{19}$$

$$\begin{aligned}\mathbf{f}^{\mathrm{b}}(\mathbf{x},t) = &\int \left(-\mathbf{f}(s,t)\right)\delta_c(\mathbf{x}-\mathbf{X}(s,t))ds + \frac{1}{2}\nabla\times\int(-\mathbf{n}(s,t))\delta_c(\mathbf{x}-\mathbf{X}(s,t))ds \\ &+ \int\left(-\mathbf{f}^{\mathrm{r}}(s,t)\right)\delta_c(\mathbf{x}-\mathbf{X}(s,t))ds,\end{aligned} \tag{20}$$

$$\frac{\partial \mathbf{X}(s,t)}{\partial t} = \int \mathbf{u}(\mathbf{x},t)\,\delta_c(\mathbf{x}-\mathbf{X}(s,t))d\mathbf{x} - \frac{1}{\alpha}\mathbf{f}(s,t), \tag{21}$$

$$\mathbf{W}(s,t) = \frac{1}{2}\int(\nabla\times\mathbf{u})(\mathbf{x},t)\delta_c(\mathbf{x}-\mathbf{X}(s,t))d\mathbf{x}, \tag{22}$$

$$\frac{\partial \mathbf{D}^i(s,t)}{\partial t} = (\mathbf{W}(s,t) - \frac{1}{\beta}n^3(s,t)\mathbf{D}^3(s,t))\times\mathbf{D}^i(s,t), \quad i=1,2,3. \tag{23}$$

Equations (12-13) are the incompressible Navier-Stokes equations written in Eulerian variables $(\mathbf{x},t)$, where $\mathbf{x}=(x_1,x_2,x_3)$ are fixed Cartesian coordinates and t is the time. The motion of the fluid is subject to the body force $\mathbf{f}^{\mathrm{b}}(\mathbf{x},t)$, which here represents the force per unit volume applied to the fluid by the immersed rod. The vector field $\mathbf{u}(\mathbf{x},t)$ is the fluid velocity and $p(\mathbf{x},t)$ is the fluid pressure. The constant parameters ρ and μ are the fluid density and the fluid viscosity, respectively.

The equilibrium equations (14-19) are employed to describe the force and torque of the immersed rod in terms of the space curve and its associated triad $(\mathbf{X}(s,t), \mathbf{D}^1(s,t), \mathbf{D}^2(s,t), \mathbf{D}^3(s,t))$. The rod deforms into an intrinsic shape determined by the intrinsic twist vector.

All variables in these equilibrium equations are functions of the material coordinate s (not necessarily arclength) and the time t. These are therefore Lagrangian variables. $\mathbf{F}(s,t)$ and $\mathbf{N}(s,t)$ are the force and moment (couple) transmitted across a section of the rod at location s at time t. These can in principle be obtained by integrating the stresses acting across that section of the rod with appropriate weight as needed to obtain the transmitted force or moment. In practice, however, the transmitted force and moment are obtained from the constitutive equations of the Kirchhoff rod, i.e., from equations (18-19). Note that these constitutive equations give the components of $\mathbf{F}$ and $\mathbf{N}$ in the basis of the triad $\{\mathbf{D}^1, \mathbf{D}^2, \mathbf{D}^3\}$. The expressions $-\mathbf{f}(s,t)ds$ and $-\mathbf{n}(s,t)ds$ are the force and torque applied by the arc ds of the rod to the fluid. (Note that $\mathbf{f}(s,t)$ and $\mathbf{n}(s,t)$ are Lagrangian variables, even though they are written as lower-case letters.)

Equations (20-22) describe the interactions between the fluid and the rod. These interaction equations connect the Lagrangian and Eulerian variables via a three-dimensional smoothed Dirac delta function $\delta_c(\mathbf{x}) = \delta_c(x_1)\delta_c(x_2)\delta_c(x_3)$, where

$$\delta_c(\mathbf{x}) = \frac{1}{c^3}\phi\left(\frac{x_1}{c}\right)\phi\left(\frac{x_2}{c}\right)\phi\left(\frac{x_3}{c}\right), \tag{24}$$

where $\mathbf{x} = (x_1, x_2, x_3)$ and the function ϕ is given by

$$\phi(r) = \begin{cases} \dfrac{3 - 2|r| + \sqrt{1 + 4|r| - 4r^2}}{8} & \text{if } |r| \le 1, \\ \dfrac{5 - 2|r| - \sqrt{-7 + 12|r| - 4r^2}}{8} & \text{if } 1 \le |r| \le 2, \\ 0 & \text{if } |r| \ge 2. \end{cases}$$

Note that $\delta_c(\mathbf{x} - \mathbf{X})$ is a continuous function of $\mathbf{x}$ with continuous first derivatives and with support equal to a cube of edge $4c$ centered on $\mathbf{X}$. Whenever c is an integer multiple of the meshwidth h, the function $\delta_c(\mathbf{x} - \mathbf{X})$ satisfies two identities as follows.

$$\sum_{\mathbf{j}} \delta_c(\mathbf{j}h - \mathbf{X})h^3 = 1, \tag{25}$$

$$\sum_{\mathbf{j}} (\mathbf{j}h - \mathbf{X})\delta_c(\mathbf{j}h - \mathbf{X})h^3 = 0, \tag{26}$$

where $\mathbf{j}$ is any vector with integer components, and h is the meshwidth of the fluid grid. Note in particular that these identities hold for all $\mathbf{X}$. As mentioned above, these identities hold only if c/h is a positive integer, and we shall choose h so that this is the case. The above identities ensure that force and torque generated by the rod are correctly applied to the fluid by our numerical scheme [31].

As stated above, the parameter c determines the spatial scale of the support of the function δ_c. It is within this support that the model flagellum averages the fluid velocity and angular velocity to determine the velocity of its centerline and the angular velocity of its triads. Likewise, it is within the support of δ_c that the model flagellum applies force and torque to the fluid. In this way, the parameter c determines the effective radius of the model flagellum, insofar as its interaction with the fluid is concerned. For validation of this concept of effective radius in immersed boundary computations involving slender immersed bodies, see [32].

In equation (20), the first term describes how to apply the force of the rod to the fluid and the second term describes how to apply the torque of the rod to the fluid. See [31] for more detailed explanation. The repulsive force $\mathbf{f}^{\mathrm{r}}$ is included to avoid penetration between two flagella. It is assumed to be a Hookean force which is applied only when the distance between the centerlines of the two flagella is less than the specified value D. This force is given by:

$$\mathbf{f}^{\mathrm{r}} = \sum_{s'} \mathbf{f}^{\mathrm{r}}(s, s', t), \tag{27}$$

where

$$\mathbf{f}^{\mathrm{r}}(s, s', t) = c_r \left(1 - \frac{|\mathbf{X}(s,t) - \mathbf{X}(s',t)|}{D}\right) \frac{\mathbf{X}(s,t) - \mathbf{X}(s',t)}{|\mathbf{X}(s,t) - \mathbf{X}(s',t)|}, \tag{28}$$

for any two material points s and s' on different flagellar filaments such that $|\mathbf{X}(s,t) - \mathbf{X}(s',t)| \leq D$. The constant D is twice the thickness of the flagellum and the constant c_r is chosen sufficiently large so that the flagella do not cross. Note that the repulsive force does not play a role in simulations of a single flagellum.

Equation (21) is the equation of motion for the centerline of a flagellum. The first term on the right-hand side is the locally averaged fluid velocity evaluated by using the smoothed Dirac delta function as a kernel, and the second term allows for slip between the flagellum and the surrounding fluid, with α as a drag coefficient. (The limit of infinite α gives the no-slip condition.) We assume an isotropic drag model in which the velocity of the flagellum

relative to that of the surrounding fluid is proportional to the force density $-\mathbf{f}(s,t)$ applied by the flagellum to the fluid.

Equation (22) defines the locally averaged angular velocity $\mathbf{W}(s,t)$ of the fluid in the neighborhood of point s of a flagellum. On the right-hand side, $\frac{1}{2}(\nabla \times \mathbf{u})(\mathbf{x},t)$ is the angular velocity of the fluid, and the smoothed Dirac delta function is again used as a kernel to define the corresponding locally averaged angular velocity.

Equation (23) states how the triads that define the material frame of a flagellum are rotated. The angular velocity of this rotation is the locally averaged angular velocity of the fluid, $\mathbf{W}(s,t)$, plus a term that allows for rotational slip about the $\mathbf{D}^3$ axis only. (Recall that $\mathbf{D}^3$ is approximately tangential to the centerline of the flagellum.) The slip angular velocity is assumed proportional to the axial component of torque density $-n^3$ applied by the flagellum to the fluid, with rotational drag coefficient β. In the limit of infinite β, the triads rotate at the locally averaged angular velocity of the fluid.

As discussed in the Introduction, we allow for translational and rotational slip only because we cannot resolve the small-scale flow patterns that occur within a flagellar bundle, once the bundle has formed. Allowing for small amounts of translational and rotational slip of the flagella relative to the fluid seems to work well with the repulsive force between filaments to prevent the filaments from crossing each other. The constants α and β were adjusted by trial and error to prevent such crossing. The values that were settled upon (see Table 1) are large (which means that the slip they allow is *small*) in the sense that they correspond to translational and rotational drag coefficients that would be expected if the radius of the flagella were on the order of $2\mu m$, which is substantially larger than the effective radius of the flagella in our simulation ($0.08\mu m$), and even more so in comparison to the radius of a real bacterial flagellum ($0.01\mu m$). We mention these numbers only to point out that the deviation from the no-slip condition that we are allowing here is a small one, yet it seems to be necessary (at current grid resolution) to achieve topologically consistent results.

III. RESULTS AND DISCUSSION

Table I shows the parameters used in this work in which the available values are chosen from the literature related to bacterial flagella such as *E. coli* and *Salmonella typhimurium*

[1, 2, 6, 9, 11–13, 33], and parameters not available in the literature are chosen by trial and error. In particular, we set all of the penalty parameters b_i equal to each other, and chose their common value such that the relative change in length of any part of any filament that occurs during our computations is no greater than 0.003. The intrinsic curvature and twist were chosen to fit the helical radius and pitch of a normal left-handed helical flagellum using the formula (10). For simplicity, we assume that the rod is isotropic in the sense that its bending modulus does not depend on the direction of the bend, so that $a_1 = a_2 = a$. Finally, we set $\kappa_2 = 0$, which implies that $\kappa = \kappa_1$.

The normal form of a flagellum of *E. coli* is a left-handed helix, and hence we use left-handed helices as intrinsic shapes except where stated otherwise. As mentioned in section II, for $\tau > 0$, the straight rod deforms into a stable left-handed helix, and for $\tau < 0$, the rod becomes a stable right-handed helix.

A. The motion of a rotating single flagellum

Figure 1 shows the initial configuration (first panel) and two snapshots of a rotating left-handed helix (second and third panels). The only difference in the setup is the direction of rotation. In the case of a left-handed flagellum turning CCW (when viewed from the non-motor end, looking back towards the motor) there is, in effect, a wave along the flagellum which propagates from its proximal end (the motor end) to its distal end (the free end). See Supplemental Material Movie 1 [34] for an animated version of this figure. There are fluid markers distributed around the flagellum in Figure 1. The fluid markers near the filament in the second panel of the figure rotate CCW along with the filament, and the fluid markers located away from the filament rotate CCW in a small circle and at the same time rotate CCW around the filament in a larger circle. The third panel of Figure 1 shows a left-handed flagellum turning CW (see Supplemental Material Movie 2 [34]). Now the helical wave propagates towards the motor instead of away from it. We observe that the helical pitch and amplitude are different from those of the left-handed helix turning CCW. This difference between the two cases illustrates the influence of fluid-dynamical forces on the configuration adopted by a rotating flagellum, since the flagellum is elastic.

By symmetry, it is obvious that a right-handed helix turning CW will behave like a left-handed helix turning CCW, and that a right-handed helix turning CCW will behave

TABLE I. *Computational and physical parameters*

Parameters	symbol	value
grid size	$N \times N \times N$	128^3
domain size	$L \times L \times L$	$L = 10\ \mu$m
axial length of the filament	ℓ	6μm
time step	$\triangle t$	1.0×10^{-7}s
fluid density	ρ	$1.0 \times 10^{-12}\ \mathrm{g}/\mu\mathrm{m}^3$
fluid viscosity	μ	$0.01 \times 10^{-4}\ \mathrm{g}/(\mu\mathrm{m} \cdot \mathrm{s})$
bending modulus	$a_1 = a_2 = a$	$3.5 \times 10^{-3}\ \mathrm{g} \cdot \mu\mathrm{m}^3/\mathrm{s}^2$
twist modulus	$a_3 = a$	$3.5 \times 10^{-3}\ \mathrm{g} \cdot \mu\mathrm{m}^3/\mathrm{s}^2$
shear force constant	$b_1 = b_2 = b$	$8.0 \times 10^{-1}\ \mathrm{g} \cdot \mu\mathrm{m}/\mathrm{s}^2$
stretch force constant	$b_3 = b$	$8.0 \times 10^{-1}\ \mathrm{g} \cdot \mu\mathrm{m}/\mathrm{s}^2$
curvatures	$\kappa_1,\ \kappa_2$	$\kappa_1 = 1.3057\mu\mathrm{m}^{-1}, \kappa_2 = 0$
intrinsic curvature	$\kappa = \sqrt{\kappa_1^2 + \kappa_2^2}$	$1.3057\mu\mathrm{m}^{-1}$
intrinsic twist density	τ	$2.1475\mu\mathrm{m}^{-1}$
translational drag coefficient	α	$2 \times 10^{-4}\ \mathrm{g}/(\mu\mathrm{m} \cdot \mathrm{s})$
rotational drag coefficient	β	$2 \times 10^{-4}\ \mathrm{g} \cdot \mu\mathrm{m}/\mathrm{s}$
effective radius of the delta function	c	0.0781μm
closest distance between two flagella	D	0.04μm
stiffness for the repulsive force	c_r	$200\mathrm{g}/\mathrm{s}^2$
motor rotation rate		100Hz
distance between two flagella motors		1.5625μm

like a left-handed helix turning CW. We have checked that our simulations respect these symmetries (data not shown).

B. Hydrodynamic interaction between two flexible flagella

Now we consider a pair of left-handed helical flagella. There are three different combinations of rotation direction: (CCW, CCW), (CCW, CW), and (CW, CW). An important question is under what conditions do the flagella wrap around each other to form a super-

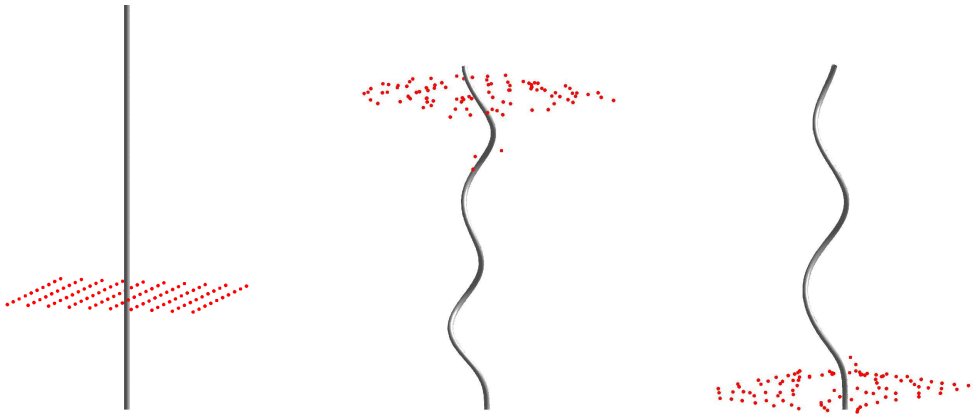

(a) Initial shape (b) CCW rotation (c) CW rotation

FIG. 1. (Color online) The initial configuration (first panel) and the motion of a left-handed helical flagellum rotated at 100Hz in the counterclockwise direction (second panel) or in the clockwise direction (third panel). The motor is at the lower end of the flagellum. In both cases, the motor end is fixed in place, and the vector $\mathbf{D}^3$ of its triad is the constant vector $(0, 0, 1)$. The vectors $\mathbf{D}^1$ and $\mathbf{D}^2$ of the motor triad rotate about $\mathbf{D}^3$ at the specified frequency and in the specified direction as stated above. The terms counterclockwise (CCW) and clockwise (CW) are defined relative to an observer looking down the z-axis, i.e., from outside the bacterium (although the bacterium itself is not explicitly modeled here). The fundamental difference between the two directions of rotation is that in the second panel the helical wave propagates away from the motor, whereas in the third panel it propagates towards the motor. Except for the motor point, which is fixed in place and rotates as prescribed above, the rest of the flagellum is free to move with the fluid. Its centerline moves approximately at the local fluid velocity, and its triads rotate approximately at the local fluid angular velocity. (Recall that we allow slip between the flagellum and the fluid.) The red particles distributed around the model flagellum are fluid markers.

flagellum as is observed in the case of *E. coli*. The two model flagella in our simulations are identical and spin side by side at the same rotation rate without any phase difference. The lateral displacement from one flagellum to the other is 1.5625 μm. In these simulations the only parameter that we vary is the direction of rotation. All other parameters are the same as in the single-flagellum case.

Figure 2 shows two left-handed flagella forming a superflagellum when the both motors spin CCW at 100Hz (see Supplemental Material Movie 3 [34]). Figure 3 shows two left-

handed flagella working independently when one of the motors spins CCW at 100Hz and the other motor spins CW at 100Hz (see Supplemental Material Movie 4 [34]). For a pair of left-handed flagella, we find that there are no other combinations of rotation directions besides CCW-CCW that result in the formation of a superflagellum. By symmetry, the above results imply that a pair of right-handed flagella spinning at the same rotation rate will form a superflagellum if and only if both flagella are spinning clockwise (when viewed from the non-motor end, looking back towards the motor). We have also considered a pair of flagella in which one is left-handed and the other is right-handed. In this case, there are no combinations of the two spinning directions in which a superflagellum forms (data not shown).

The above results may be summarized as follows. Two identical (possibly mirror-image) flagella spinning side by side at the same rotation rate will form a superflagellum if and only if *both* of the following two conditions are met:

1. The two flagella have the same handedness.

2. The direction of spin of each flagellum is such that the helical wave progresses along it from the motor end towards the non-motor end.

We have also investigated what happens if the two motors run at different speeds. Consider two left-handed flagella spinning side by side, both in the counterclockwise direction, at *almost* the same rotation rate. For example, let one of them spin at 100 Hz and the other at 102 Hz. What happens is that a superflagellum initially forms just as though the rotation rates were identical, but the superflagellum only lasts for a finite time and then falls apart, see Figure 4 (see Supplemental Material Movie 5 [34]). We have observed a linear relationship (data not shown) between the lifetime of the superflagellum and the reciprocal of the frequency difference. These results suggest that an exact match of rotation rates is required for the formation of a permanent superflagellum, and they raise the question how can nature achieve such precision? This issue is resolved by noting an unrealistic feature of our model, that the rotation rate of the motor is prescribed, independent of load. The angular velocity of an actual bacterial flagellar motor is load-dependent [1, 35]. This will result in a hydrodynamic interaction between the motors of flagella that are forming a bundle, and one can guess that this interaction will tend to synchronize the motors, so that even if their

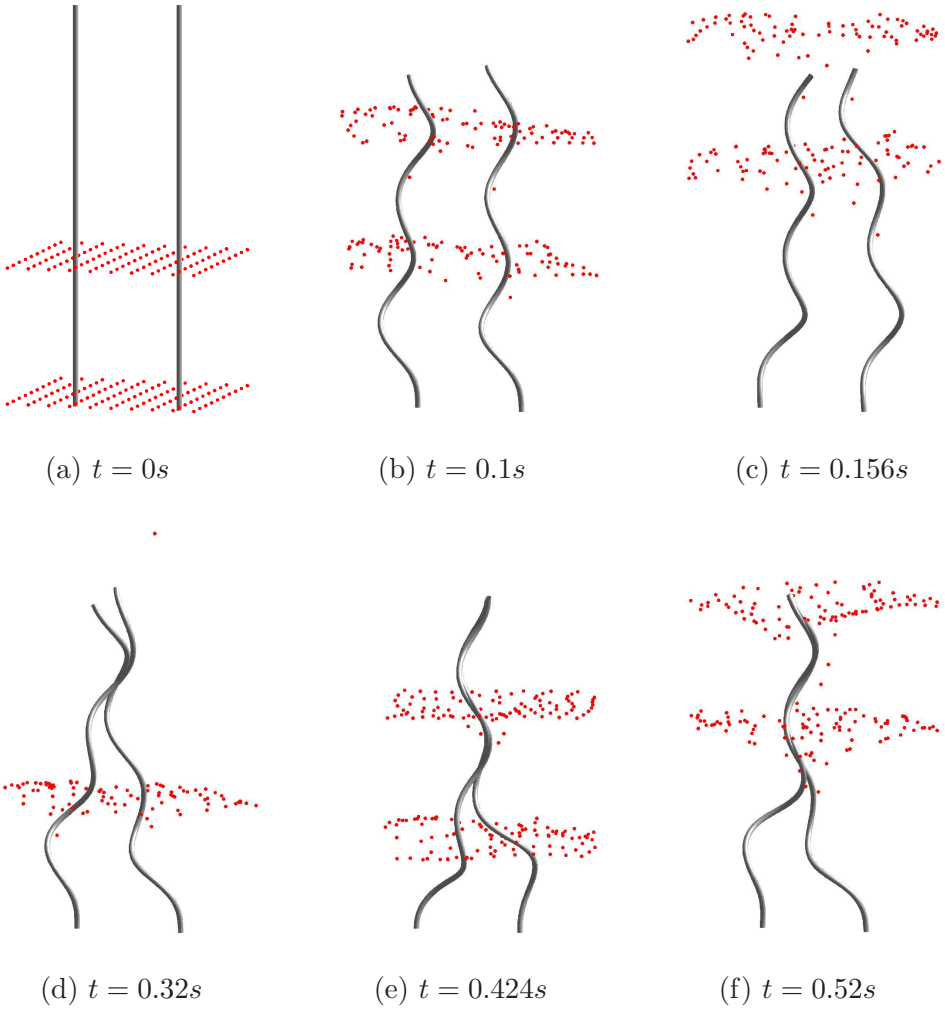

(a) $t = 0s$ (b) $t = 0.1s$ (c) $t = 0.156s$

(d) $t = 0.32s$ (e) $t = 0.424s$ (f) $t = 0.52s$

FIG. 2. (Color online) Bundling process viewed from the side. Hydrodynamic interaction between two left-handed helical flagella when both motors turn CCW at 100Hz. The time t of each frame is noted below that frame. Flagella are straight at $t = 0$ but quickly evolve towards their intrinsic, helical shape. Red particles are fluid markers which move at the local fluid velocity. The initial positions of these markers are in two horizontal planes and another set of fluid markers appears at times $t = 0.2s$ and $0.4s$.

intrinsic rotation rates are slightly different, they will coordinate as their flagella bundle into a superflagellum. This conjecture will be checked in future work.

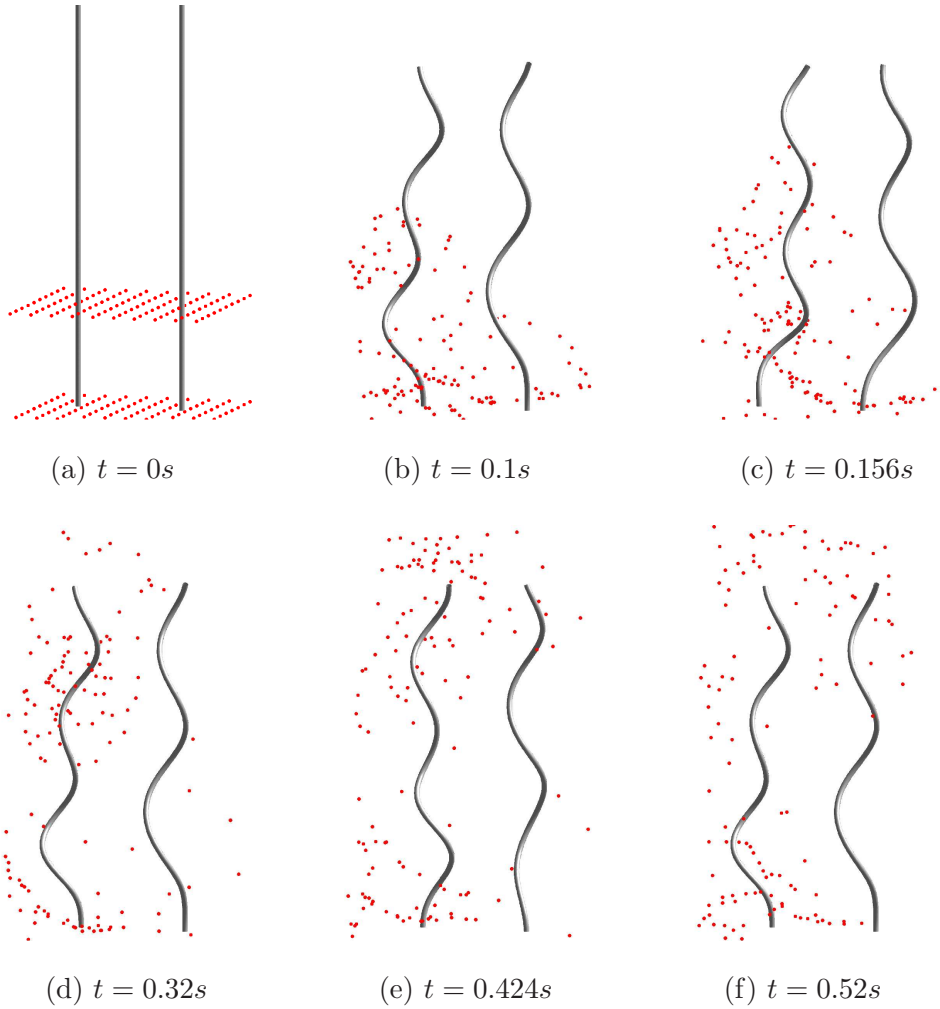

(a) $t = 0s$ (b) $t = 0.1s$ (c) $t = 0.156s$

(d) $t = 0.32s$ (e) $t = 0.424s$ (f) $t = 0.52s$

FIG. 3. (Color online) Hydrodynamic interaction between two left-handed helical flagella when one of the motors turns CCW at 100Hz and the other motor turns CW at 100Hz.

IV. CONCLUSION

Our computational model describes a pair of micron-scale flexible bacterial flagella interacting with an incompressible viscous fluid. The fluid-mechanical interplay between the two flagella may result in flagellar bundling, depending on the handedness of the helices and the direction of rotation of the flagellar motors. In particular, we have found that bundling only occurs if the two flagella have the same handedness, and only if they both turn in the direction that makes the helical wave on each flagellum propagate from the motor end towards the non-motor end (i.e., away from the body of the bacterium to which the flagella are attached). We have checked that the violation of either of these criteria is enough to prevent bundling, even when the other one is satisfied. Thus flagella of opposite handedness

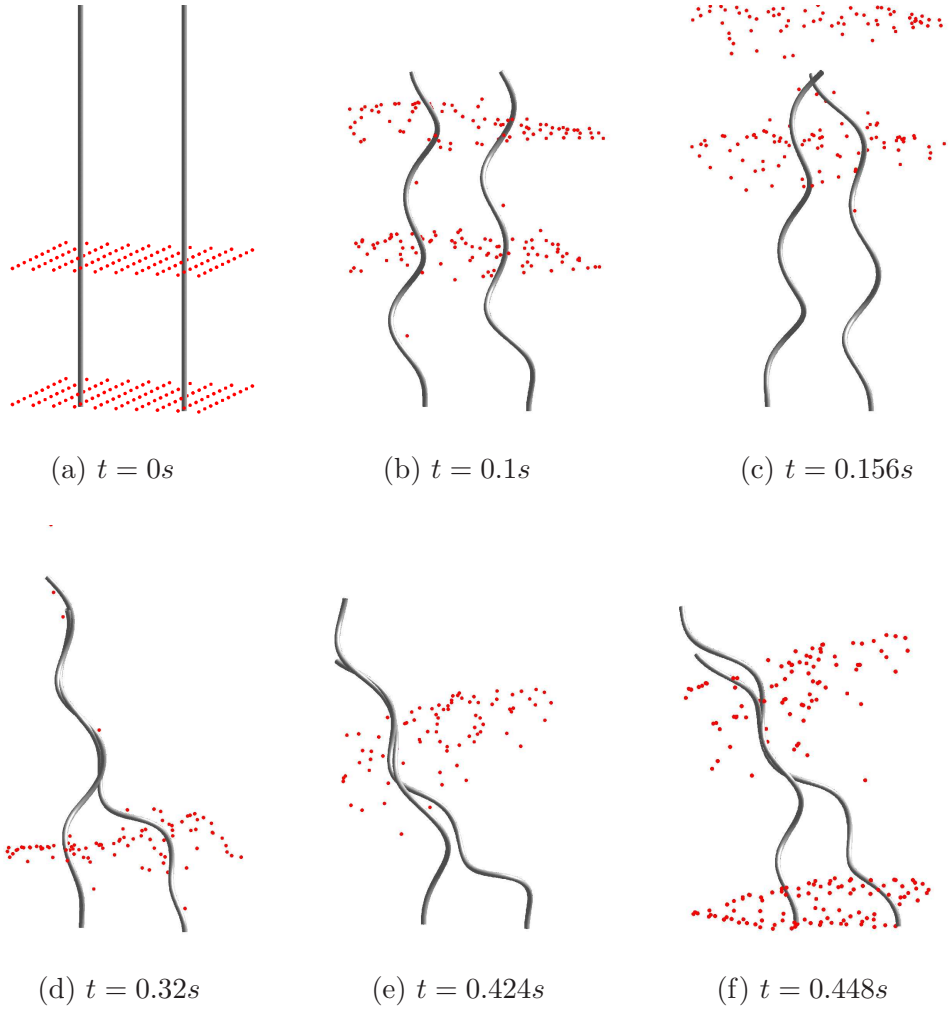

(a) $t = 0s$ (b) $t = 0.1s$ (c) $t = 0.156s$

(d) $t = 0.32s$ (e) $t = 0.424s$ (f) $t = 0.448s$

FIG. 4. (Color online) Hydrodynamic interaction between two left-handed helical flagella when one of the motors turns CCW at 100Hz and the other motor turns CCW at 102Hz.

do not bundle, regardless of their directions of rotation, and flagella of the same handedness that spin in the same direction do not bundle if the direction of spin makes a helical wave that propagates towards the motors instead of away from them.

There are many ways in which the model of this paper can be extended and improved, and these will be the subject of future work. With regard to the flagella themselves, we thank an anonymous reviewer for pointing out that each flagellum in reality is connected to its motor by a "hook" that acts as a universal joint [36, 37]. This feature should be included in future versions of the model. We also plan to study the effects of polymorphic transitions, which can be included in the model by the use of energy functions with several local minima. It will be especially interesting to study the effects of fluid mechanical forces on such transitions,

and the effects of such transitions on the bundling and unbundling processes. With regard to the flagellar bundle, it is obviously important to consider more than two flagella, and we think it will also be important to resolve the fluid flows within the bundle itself. An adaptive version of the generalized IB method of the present paper has been developed [38]. This adaptive methodology, which has been implemented within the open-source IBAMR software [39], seems well suited to resolving the details of flow within a flagellar bundle. The influence of bundling on the energetics of pumping fluid remains to be elucidated, and the optimization of flagellar parameters to promote bundling and ultimately to pump fluid is an open problem. Since bundling seems to be critically dependent upon synchronization, it will be important to study motors which do not rotate at a prescribed rate, but instead have a rotation rate that depends in a realistic way upon the load. Finally, the influence of the bacterium itself on the bundling of its flagella should be considered. Thus, bundling should be modeled in the context of a freely swimming bacterium, which the flagella propel, and to which they are attached. Both the surface of the bacterium acting as a boundary, and also the motion of the bacterium through the surrounding fluid may have a profound influence as noted by Anderson [4], who pointed out that the motion of the bacterium through the fluid may help "sweep" the flagella into a bundle, and that the counter-rotation of the bacterium during swimming may help "twist" the flagella into a bundle. The methods of this paper are well suited to the study of all of these problems.

ACKNOWLEDGMENTS

We would like to thank H. Berg, T. Powers, and P. Holmes for helpful discussions. This work was supported by National Science Foundation Grant DMS-0815751 and Charles Phelps Taft Research Center, University of Cincinnati.

---

[1] H. C. Berg, Annu. Rev. Biochem. **72**, 19 (2003).

[2] R. M. Berry, *Bacterial flagella: Flagellar motor, Encyclopedia of life sciences* (Nature Publishing Group, 2005).

[3] R. M. Macnab, "Escherichia coli and salmonella," (Washington, DC, 1996) pp. 123–145.

[4] R. A. Anderson, "Formation of the bacterial flagellar bundle," (New York, London: Plenum Press, 1974).

[5] A. Arkhipov, P. L. Freddolino, K. Imada, K. Namba, and K. Schulten, Biophysical Journal **91**, 4589 (2006).

[6] N. C. Darnton and H. C. Berg, Biophysical Journal **92**, 2230 (2007).

[7] H. Flores, E. Lobaton, S. Mendez-Diez, S. Tlupova, and R. Cortez, Bulletin of Mathematical Biology **67**, 137 (2005).

[8] J. J. L. Higdon, J. Fluid Mech. **94**, 331 (1979).

[9] M. J. Kim, J. C. Bird, A. J. V. Parys, K. S. Breuer, and T. R. Powers, Proc. Natl. Acad. Sci. **100 (26)**, 15481 (2003).

[10] M. Ramia, D. L. Tullock, and N. Phan-Thien, Biophys. J. **65**, 755 (1993).

[11] L. Turner, W. S. Ryu, and H. C. Berg, J. of Bacteriology **182 (10)**, 2793 (2000).

[12] H. Wada and R. R. Netz, EPL **82**, 28001 (2008).

[13] J. W. McClaine and R. M. Ford, Appl. Environ. Microbiol. **68**, 1280 (2002).

[14] R. Kamiya and S. Asakura, J. Mol. Biol. **106**, 167 (1976).

[15] R. Kamiya and S. Asakura, J. Mol. Biol. **108**, 513 (1977).

[16] R. M. Macnab and M. K. Ornston, J. Mol. Biol. **112**, 1 (1977).

[17] E. Hasegawa, R. Kamiya, and S. Asakura, J. Mol. Biol. **160**, 609 (1982).

[18] H. Hotani, J. Mol. Biol. **156**, 791 (1982).

[19] G. I. Taylor, Proc. Roy. Soc. Lon. Ser. A **209 (1099)**, 447 (1951).

[20] G. I. Taylor, Proc. Roy. Soc. Lon. Ser. A **211 (1105)**, 225 (1952).

[21] N. Chouaieb, A. Goriely, and J. H. Maddocks, Proc. Natl. Acad. Sci. U.S.A. **103 (25)**, 9398 (2006).

[22] S. Lim, Physics of Fluid **22**, 024104 (2010).

[23] R. Dillon, L. Fauci, and D. G. III, J. Theor. Biol. **177**, 325 (1995).

[24] L. Fauci and C. S. Peskin, J. Comput. Phys. **77**, 85 (1988).

[25] A. L. Fogelson, J. Comput. Phys. **56**, 111 (1984).

[26] E. Jung and C. S. Peskin, SIAM J. Sci. Comput. **23**, 19 (2001).

[27] S. Lim and C. S. Peskin, SIAM J. Sci. Comput. **25**, 2066 (2004).

[28] L. A. Miller and C. S. Peskin, J. Exp. Biol. **208(Pt.2)**, 195 (2005).

[29] K. Rejniak, H. Kliman, and L. Fauci, Bulletin of Math Biology **66**, 199 (2004).

[30] L. Zhu and C. S. Peskin, J. Comput. Phys. **179**, 452 (2002).

[31] S. Lim, A. Ferent, X. S. Wang, and C. S. Peskin, SIAM J. Sci. Comput. **31 (1)**, 273 (2008).

[32] T. T. Bringley and C. S. Peskin, J. Comput. Phys. **227 (11)**, 5397 (2008).

[33] C. R. Calladine, J. Mol. Biol. **118**, 457 (1978).

[34] See Supplemental Material at [URL will be inserted by publisher] for animated versions of Figures 1(b), 1(c), 2, 3 and 4 (2012).

[35] C. V. Gabel and H. C. Berg, Proc. Natl. Acad. Sci. **100 (15)**, 8748 (2003).

[36] H. C. Berg, Biophys. J. **68**, 163s (1995).

[37] F. A. Samatey, H. Matsunami, K. Imada, S. Nagashima, T. R. Shaikh, D. R. Thomas, J. Z. Chen, D. J. DeRosier, A. Kitao, and K. Namba, Nature **431**, 1062 (2004).

[38] B. E. Griffith and S. Lim, Comm. Comput. Physics **12(2)**, 433 (2012).

[39] IBAMR, http://ibamr.googlecode.com.